Received: 13 June 2017 | Revised: 01 September 2017 | Accepted: 29 November 2017 | Published on: 25 January 2018

DOI: 10.1002/qj.3218

Quarterly Journal of the Royal Meteorological Society RMetS

Evaluation of diurnal variation of GPM IMERG-derived summer precipitation over the contiguous US using MRMS data

Sungmin O[1,2] | Pierre-Emmanuel Kirstetter[3,4,5]

[1]IGAM/IP, NAWI Graz, University of Graz, Austria
[2]DK Climate Change, University of Graz, Austria
[3]Advanced Radar Research Center, University of Oklahoma, Norman, Oklahoma
[4]NOAA/National Severe Storms Laboratory, Norman, Oklahoma
[5]School of Civil Engineering and Environmental Science, University of Oklahoma, Norman, Oklahoma

Correspondence
P.-E. Kirstetter, Advanced Radar Research Center, 120 David L. Boren Blvd, Norman, OK.
Email: pierre.kirstetter@noaa.gov

This paper investigates the accuracy of the Integrated Multi-satellitE Retrievals for Global Precipitation Measurement (GPM), which provides merged microwave and infrared satellite precipitation estimates, over the contiguous US. The study focuses on diurnal variations in precipitation during a two-year summer period (June–August, 2014–2015). The normalized amplitude and phase of the diurnal cycle of IMERG are evaluated against those of ground reference from the Multi-Radar/Multi-Sensor system in terms of precipitation amount, frequency and intensity on a 1°/1 hr scale. IMERG well captures large-scale regional features of the diurnal cycle of precipitation and overall agrees well with the reference for both diurnal and semidiurnal variations. The comparison results indicate that the IMERG precipitation estimates can be a reliable alternative to ground-based measurements even at the subdaily scale; however, region-specific data discrepancies are still observed. For instance, we reveal that IMERG substantially overestimates normalized amplitude of diurnal precipitation in the central US, while IMERG tends to underestimate diurnal variations over the mountain regions in the western and eastern US. In terms of phase, we find a significant difference in the timing of peak precipitation between convective and stratiform regions of mesoscale convective systems (MCSs) over the Great Plains. This time shift is more apparent during the mature and dissipation stages of MCSs, which lead to relatively early peaks in the diurnal cycle of precipitation from IMERG. This phase bias implies a higher sensitivity of IMERG towards the convective regions of MCSs, supposedly because of the brightness temperature depression coming from ice particles aloft sampled by spaceborne passive microwave sensors. Such discrepancy between the actual and satellite-estimated precipitation timing can be challenging, e.g. when the satellite data are used to study subdaily precipitation processes or to validate numerical simulations. Consequently, our assessment of the IMERG performances highlights the need for improvements in the IMERG system.

KEYWORDS

convective and stratiform, diurnal cycle, ground validation, mesoscale convective system, remote sensing, satellite observations

1 | INTRODUCTION

Weather satellites have become a major data source to obtain precipitation observation products at large scales for meteorological and hydrological research and operations (Hong, Adler, & Huffman, 2006; Hong, Adler, Hossain, Curtis, & Huffman, 2007; Nesbitt & Zipser, 2003; Pu et al., 2002; Zhou, Lau, & Huffman, 2015). Satellites have a unique advantage of observing precipitation over the globe, including areas where adequate ground instruments are sparse or absent. However, the indirect nature of their measurements requires that satellite estimates be validated using ground reference. The ground reference is mainly sourced from ground-based radar or rain-gauge measurements to assess the satellite estimates by identifying discrepancies between the data.

In early 2014, the National Aeronautic and Space Administration (NASA) and the Japan Aerospace Exploration Agency (JAXA) launched the Global Precipitation Measurement (GPM) mission to provide observation continuity to its predecessor, the Tropical Rainfall Measuring Mission (TRMM), and to advance satellite-based precipitation measurements with the aid of a constellation of partner satellites (Hou et al., 2014; Skofronick-Jackson et al., 2016). Since then, great efforts have been directed to evaluating the precipitation products of the GPM (e.g. Kim, Park, Baik, & Choi, 2017; Le, Chandrasekar, & Biswas, 2016; Prakash et al., 2016; O et al., 2017; Tan, Petersen, & Tokay, 2016; Tang, Ma, Long, Zhong, & Hong, 2016, and many other ongoing studies) to study their accuracy and uncertainties. Now the GPM products are expected to be extensively used over the next decades for data applications such as weather forecasting, hydrological research and climate modelling. In this study, we evaluate the Integrated Multi-satellitE Retrievals for GPM (IMERG, version 04 Final run; Huffman et al., 2015a; Huffman, Bolvin, & Nelkin, 2015b) over the contiguous United States (CONUS; Figure 1) for a two-year summer period (June–August, JJA, of 2014–2015).

Recent high-resolution satellite precipitation products like IMERG (0.1°/30 min) are broadening the use of satellite-based precipitation data on regional to local scales (Artan et al., 2007; Li et al., 2009, 2017; Pu et al., 2002). At the same time, there are concerns about possibly larger errors associated with satellite retrieval at finer resolution. This has resulted in a number of studies focusing on error characteristics of the satellite estimates at various spatial and temporal scales (Li, Zhang, & Xu, 2012; Tang et al., 2016; Tian, Peters-Lidard, Choudhury, & Garcia, 2007; Wang & Wolff, 2010; Zeweldi & Gebremichael, 2009). Here we analyze the accuracy of IMERG at a meteorologically relevant scale (1°/1 h), with emphasis on diurnal variations of precipitation. Analyzing satellite-based precipitation estimates on a diurnal basis can highlight subdaily precipitation features which can explain bias in precipitation amounts for reliable hydrological applications (e.g. rainfall–runoff modelling, flood forecasting), and also bias in diurnal timing for

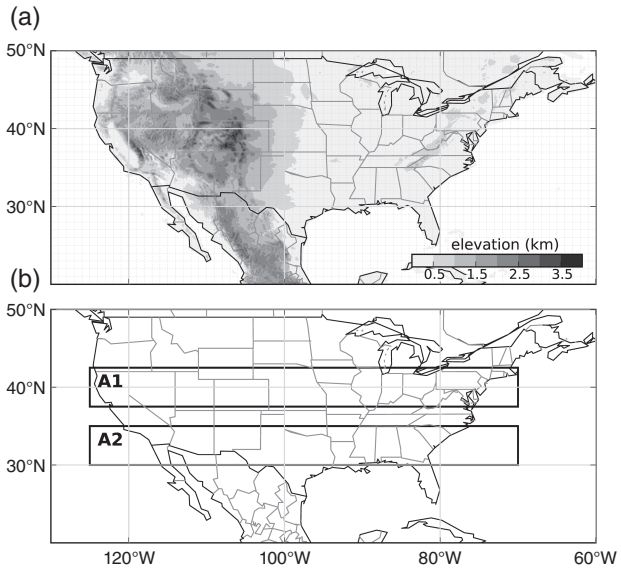

FIGURE 1 (a) The study domain and (b) the selected areas for Figures 6 and 7 (A1 and A2, respectively), and for Figure 10 (A1)

better investigation of cloud–precipitation processes (e.g. for representation of convection in global and regional climate models). Moreover, the revealed errors can be related to the physical precipitation processes involved, and hence we can address diverse accuracy requirements for different data applications. IMERG provides precipitation information suitable for deriving diurnal features on an hourly basis, whereas many other satellite data are restricted to their native time resolution (e.g. once per 3 h) or are interpolated to shorter time-scales. Accordingly, the ground reference used in this study is computed from the high-resolution (0.01°/2 min) gauge-corrected radar quantitative precipitation estimation (QPE) of the Multi-Radar/Multi-Sensor (MRMS) system (Zhang et al., 2016). We upscaled and matched the MRMS data at the IMERG spatiotemporal resolution and recalibrated with hourly gauge data for direct pixel-by-pixel comparison with IMERG. The matched dataset yielded a sufficient number of collocated IMERG-MRMS samples over diverse hydroclimatic regions of the CONUS, including mountain areas, from which robust reference diurnal precipitation patterns could be derived (section 2.2). Furthermore, the precipitation reference included precipitation type information, i.e. convective and stratiform, along with the QPE values, so we utilized this information for a detailed analysis of diurnal typology of precipitation. This enabled us to examine the satellite precipitation estimation related to rain processes to analyze possible reasons for any discrepancy between IMERG and the reference. Consequently, our results may advise caution for satellite data users and suggest further improvement areas in precipitation retrieval for developers.

The article is organized as follows. Section 2 describes the datasets and the analysis method. The overall performance of IMERG in describing diurnal precipitation variations against the reference is addressed in section 3, with a brief review of observed (semi-)diurnal precipitation cycles over the US. The

biases found from the comparison of normalized amplitude and phase of the diurnal precipitation cycles are investigated in detail in section 4. Conclusions are given in section 5.

2 | DATA AND METHOD

2.1 | GPM IMERG

GPM IMERG provides quasi-global (60°N–60°S) gridded precipitation estimates with 0.1°/30 min resolution. To generate continuous precipitation estimates, IMERG acquires the passive microwave (PMW) measurements from as many low-Earth-orbit satellites as available, and fills in temporal gaps with infrared (IR) measurements from geostationary satellites. Complete speciation of the algorithm and data can be found at Huffman et al. (2015a, 2015b). Briefly, IMERG is a unified algorithm of: (i) the NASA TRMM Multisatellite Precipitation Analysis (TMPA) for inter-satellite calibration and gauge adjustment (Huffman et al., 2007), (ii) the National Oceanic and Atmospheric Administration (NOAA) Climate Prediction Center morphing technique with Kalman filter (CMORPH-KF) for time interpolation of PMW-based estimates (Joyce & Xie, 2011), and (iii) the University of California (Irvine) Precipitation Estimation from Remotely Sensed Information using Artificial Neural Networks – Cloud Classification System (PERSIANN-CCS) for retrieval of microwave calibrated IR estimates (Hong et al., 2004). IMERG is run with multiple latencies to address different user needs (Huffman et al., 2015b). Here we consider IMERG version 04 Final run. Final run takes longer time to be processed (about 3 months) as it combines monthly gauge analysis for bias correction. All GPM products including IMERG data are available at the NASA/PMM website (https://pmm.nasa.gov/gpm; accessed 16 December 2017).

2.2 | Surface reference

The MRMS system designed by NOAA/National Severe Storms Laboratory (NSSL) integrates about 180 operational US WSR-88D weather radars, hourly gauge observations, and model analyses to create gridded precipitation products (Zhang et al., 2016). From quality-controlled radar reflectivity data interpolated onto a 3D grid and environmental field, precipitation type (e.g. stratiform, convective, and snow) and surface rates are derived at each grid point every 2 min. A Radar Quality Index (RQI; Zhang, Qi, Howard, Langston, & Kaney, 2011) indicates the precipitation rate estimation uncertainty relative to the radar sampling, such as beam blockage and phase of precipitation. Convective areas are identified by analysing the spatial structure of the vertically integrated liquid (VIL) content. At the hourly time-scale, the precipitation rates are adjusted using gauge networks.

Kirstetter et al. (2012) demonstrated the use of MRMS precipitation products for comparison with satellite estimates provided that significant gauge-based adjustments and conservative quality controls (e.g. based on RQI) are applied to derive robust and accurate precipitation estimates at the satellite pixel scale. This post-processing decreases the availability of reference precipitation data in challenging conditions like complex terrain and frozen precipitation, but increases the homogeneity of quality over the CONUS. For this analysis we use a reference derived from the MRMS suite for satellite ground validation (Gebregiorgis et al., 2017; Kirstetter et al., 2012, 2013, 2014). To facilitate the comparison on a pixel-by-pixel basis, the MRMS data are aggregated into the IMERG pixel grid (0.1°×0.1°) by averaging best quality data. Pixels having less than 75% of best-quality data are discarded and only the most trustworthy precipitation estimates are kept to compute the areal averages.

2.3 | Analysis method

The methodology applies a harmonic analysis to the diurnal precipitation cycle sampled from space and ground (as applied in Dai, 2001; Fenta, Rientjes, Haile, & Reggiani, 2014; He et al., 2015). For each 1° lat/lon grid box, the JJA averages of hourly precipitation amount (defined as the mean precipitation including zero values), frequency (the mean percentage of precipitation occurrence), and intensity (the mean of measurable precipitation, i.e. data $> 0\,\mathrm{mm\,h^{-1}}$) for IMERG and reference are computed. More than 10 800 collocated IMERG–reference pairs are obtained on average per grid per hour, which is equivalent to 59% of total potential pairs over the study period. The hourly occurrence (in percent) of convective and stratiform precipitation is also computed from the reference. As a result, empirical diurnal histograms (hourly) are derived for each quantity. Harmonic functions are fitted on the histograms using a least-squared-error method, and diurnal cycle parameters such as amplitude and phase (peak timing) are extracted from the functions. Let the fitted diurnal cycle be represented as follows:

$$P(t) = P_o + \sum_{k=1}^{N} A_k \cos\left(\frac{2k\pi}{24}t - \sigma_k\right) + \text{residual}, \qquad (1)$$

where P_o is the daily mean of the diurnal cycle, A_k and σ_k are the diurnal amplitude (the peak-to-peak amplitude is $2A_k$) and phase of the kth harmonic, and t is time in hours. This study considers the first two harmonic components, i.e. diurnal (S1, 24 h cycle) and semidiurnal (S2, 12 h cycle) harmonics. Although including the higher-order harmonics can improve the quality of the fit and decrease the residual, only the first two harmonics are commonly used for the analysis of precipitation diurnal cycles since most variability can be explained by those two harmonics (Dai, 2001; Oki & Musiake, 1994; Yin, Chen, & Xie, 2009, also section 3.1).

Previous studies using surface observations suggest that daytime insolation is the primary driving force of the S1 precipitation cycle (Dai, 2001; Yin et al., 2009). The solar heating on the ground directly relates to convective available

potential energy, which contributes to the late-afternoon precipitation maximum. However, various exceptions are found like nocturnal rainfall maxima associated with MCSs (Houze, 2004) over the CONUS (Carbone & Tuttle, 2008; Dai, Giorgi, & Trenberth, 1999; Tian, Held, Lau, & Soden, 2005), and indeed convective parametrization schemes in numerical models have difficulties in replicating accurate diurnal precipitation signals of MCSs (Clark, Gallus, & Chen, 2007; Liang, 2004; Surcel, Berenguer, & Zawadzki, 2010; Tao et al., 2013). Meanwhile, mechanisms behind S2 cycle have rarely been discussed partly due to low temporal resolution of precipitation data to resolve the S2 harmonic. Nevertheless, Dai (2001), for instance, found that the S2 cycle is more significant over the oceans and consistent with the phase of semidiurnal atmospheric tides, and Huang and Chan (2011) proposed that the S2 variation over southeast China is induced by land–sea differential heating.

3 | COMPARISON OF IMERG AND REFERENCE

3.1 | Significance of the S1 and S2 harmonics

Figure 2 shows the significance of the S1 and S2 harmonics in representing diurnal variations. The significance can be determined as the percentage of total daily variance explained by harmonic components, i.e. the variance of harmonic(s) divided by the variance of observations (Fenta et al., 2014). Note that the missing values over the Rockies are due to the quality filtering during the reference data preparation. For both IMERG and reference, S1 dominates the subdaily variation over most areas. S1 accounts for 47% and 52% on average (max 91% and 97%), while S2 accounts for around 16% and 18% (max 82% and 80%) of the diurnal variance for IMERG and reference, respectively. Thus the S1 and S2 harmonics together explain over 63% and 70% of the diurnal variance of observed precipitation for IMERG and reference, respectively.

For both IMERG and reference, high percentages of the S1 can be found over the east of the Rocky Mountains and adjacent Great Plains and the southeastern US. As a consequence of the general agreement, the correlation coefficient (Pearson's r) of the S1 between the two data is 0.68. Meanwhile, the explained percentages of variance by the S1 are much lower over regions where lower precipitation amounts fall during the summer months (e.g. the west coast) and where the diurnal cycle is weak due to other harmonics (e.g. along a diagonal band stretching northeastwards from the south central US (Texas)). This result agrees with Carbone and Tuttle (2008), who compared the standard deviation of the diurnal maximum over different regions in the US using data from ground-based radars.

The percentages of S2 are considerably lower than those of the S1. However, some regions on the diagonal band, such as Texas, Arkansas and Indiana, show that the S2 accounts for a relatively higher fraction of the diurnal variance. Although S2 agrees poorly (r= 0.52) between data, IMERG visually demonstrates the broad agreement with the reference. The explained percentages of diurnal variance by the S1 and S2

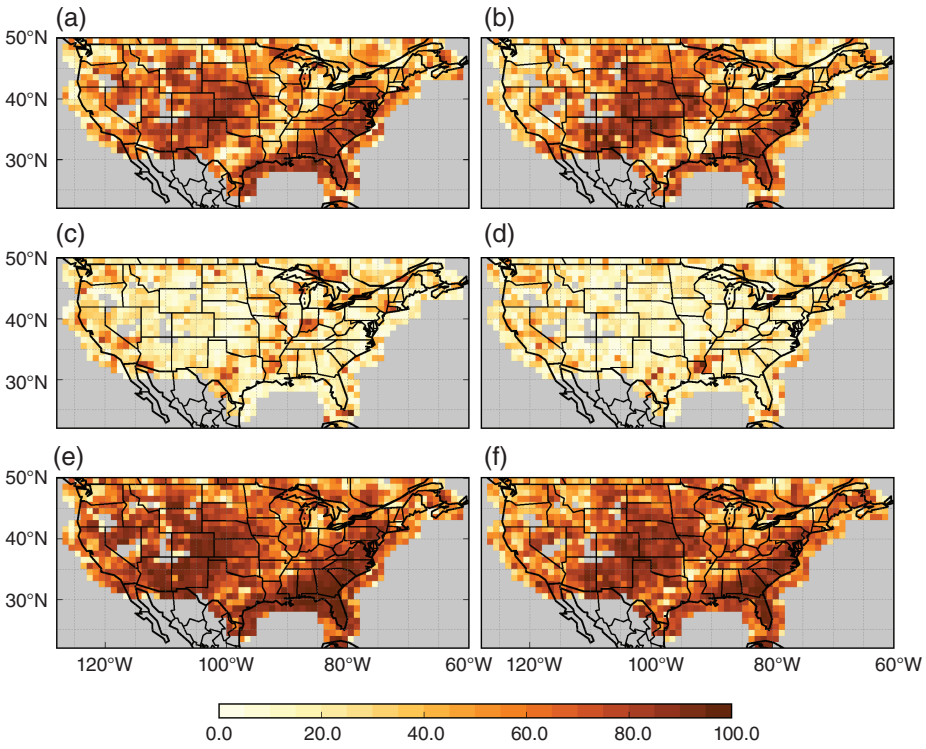

FIGURE 2 Percentage of the mean daily precipitation variance explained by the (a, b) diurnal (S1) and (c, d) semidiurnal (S2) components, and (e, f) the combined two harmonics (S1+S2) for (a, c, e) the reference and (b, d, f) IMERG

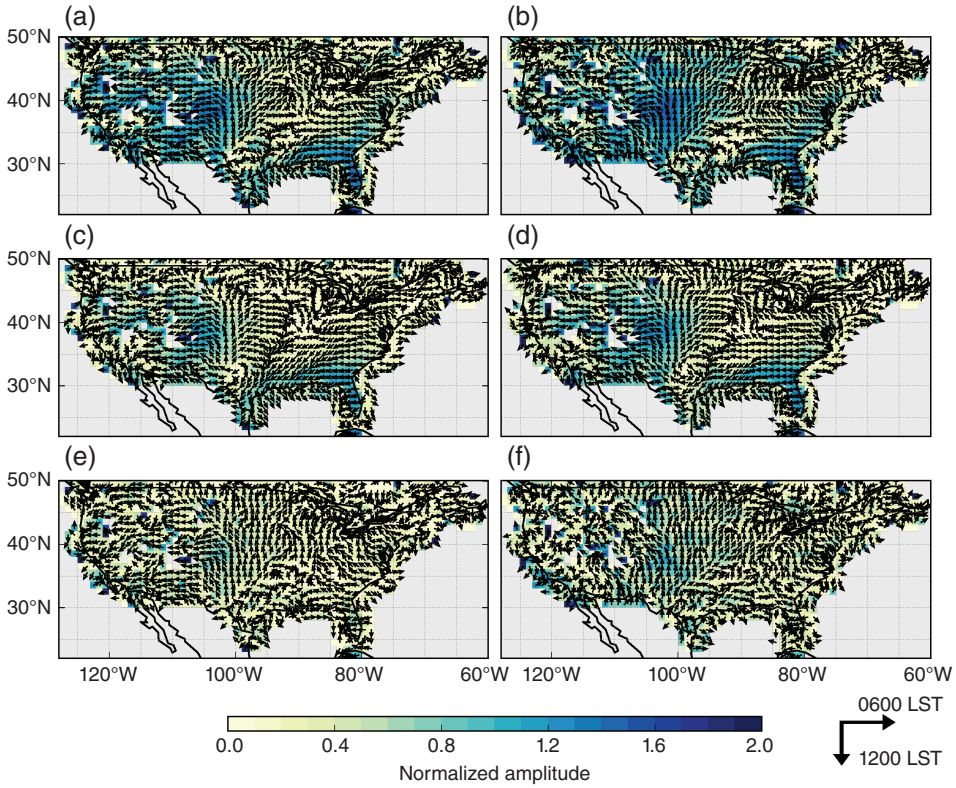

FIGURE 3 Diurnal cycles (S1) of precipitation (a, b) amount, (c, d) frequency, and (e, f) intensity derived from (a, c, e) the reference and (b, d, f) IMERG. The colour levels represent the ratio of the diurnal harmonic amplitude to the daily mean. The direction to which an arrow points indicates the local time at which the phase peak occurs (e.g. north = 0000 LST, east = 0600 LST)

for precipitation frequency give similar results (not shown) to those for precipitation amount.

3.2 | S1 and S2 precipitation cycles

Figure 3 shows the amplitude and phase of S1 cycles, in 1° × 1° grid boxes, representing precipitation amount, frequency, and intensity, derived from IMERG and the reference. Note that the amplitude is normalized by the daily mean. The normalized amplitude of S1 precipitation cycles ranges from about 60% to 200% of the daily mean. Summer precipitation in the central and southeastern US is characterized by a significant diurnal variation with amplitudes over 100% of the daily mean. IMERG fairly well describes this regional feature, although the higher-amplitude area appears wider over the Great Plains.

The reference shows that the spatial distribution of precipitation amount comes mostly from frequency rather than intensity, while precipitation intensity presents smoother geographical variations. This feature is also clearly seen in IMERG. The intensity of precipitation has much weaker amplitudes (compared to the amount and frequency) at most of the grid boxes, which implies that intensity might be not a fair indicator for satellite validation purposes, especially on a local scale. It is consistent with previous studies which found that rainfall intensity is a less prominent characteristic of the diurnal cycle in precipitation (Dai et al., 1999; Koo & Hong, 2010; Oki & Musiake, 1994; Zhou et al., 2008). The pattern correlation coefficients between IMERG and reference are 0.75, 0.80, and 0.61 for precipitation amount, frequency and intensity, respectively.

In addition to the diurnal amplitude, IMERG well reproduces the large-scale spatial pattern of diurnal phases detected by reference, e.g. late afternoon to early evening peak in most regions, and nocturnal to morning maxima over the Great Plains. IMERG also well captures local features such as morning peaks over the Gulf of Mexico/southeast US, which may be linked to sea-breeze circulations (Huang & Chan, 2011; Tian et al., 2005). Meanwhile, over the area with weaker S1 signal (e.g. the west coast and the diagonal band; Figure 2), the diurnal phase is more varied, which can be interpreted as more uncertainty in describing the diurnal precipitation variation. Agreement between IMERG and the reference over this region is poor. In general, the phase map of precipitation amount and frequency of IMERG is comparable to that of the reference. However, the peak time of precipitation intensity has a strong spatial gradient, except in the central US, particularly in IMERG, which results in a poorer agreement for the intensity between IMERG and reference.

The normalized amplitude and phase of IMERG and the reference S2 cycles are shown in Figure 4. Note that the plot scale used for the S2 amplitudes ranges from 0 to 100% (i.e. half of the S1 amplitudes) and that the peak times are within the period between 0000 and 1200 LST. A fitted semidiurnal

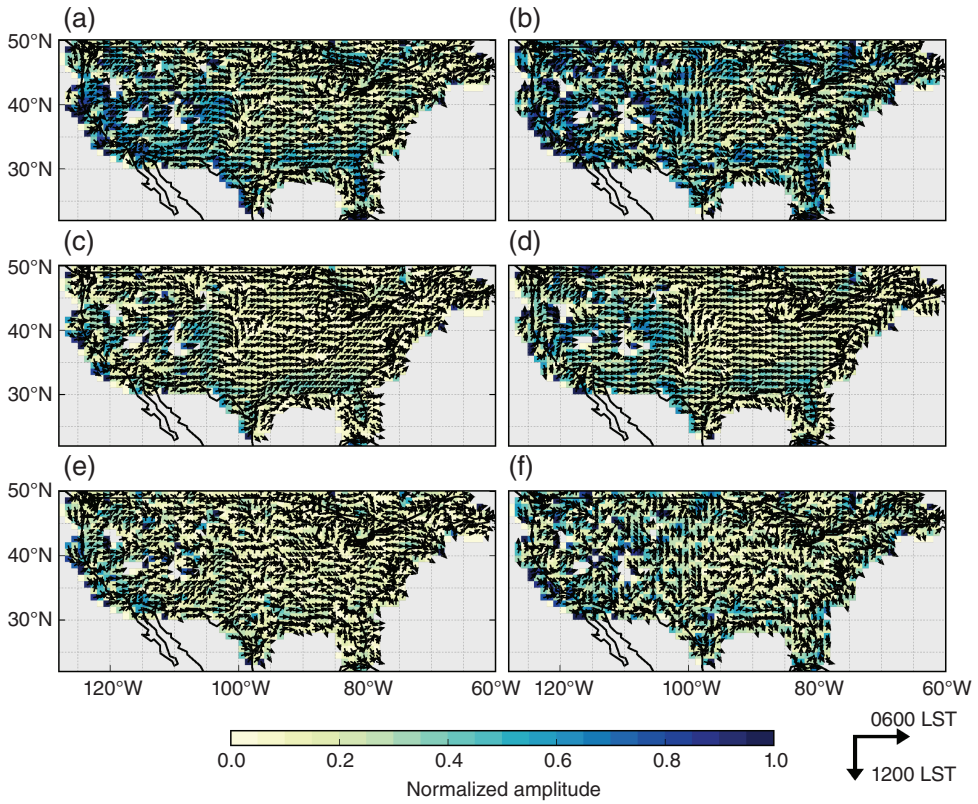

FIGURE 4 As Figure 3, but for semidiurnal precipitation cycles (S2)

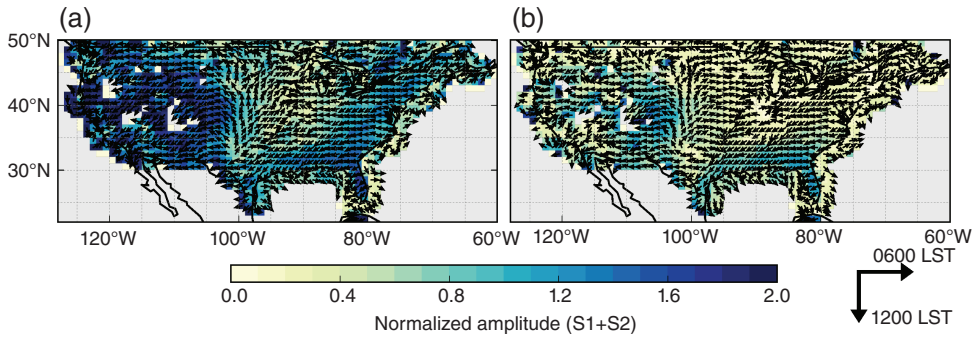

FIGURE 5 As Figure 3, but for (S1+S2) cycles of (a) convective and (b) stratiform precipitation occurrence derived from the reference

cycle peaks twice a day with a 12 h interval; for example, the grid with a 0300 LST rainfall peak means it has another peak at 1500 LST. In contrast to the S1 cycles, the regional feature of S2 cycles is less evident. Nevertheless, both IMERG and the reference depict higher S2 amplitudes over coastal regions and over the Rockies, suggesting the possibility of local effects such as land–sea or mountain–valley breezes in the secondary precipitation peak. Although IMERG shows relatively poor data agreement with the reference for S2 than for S1, IMERG spatial features still largely resemble those of the reference S2 cycles. Again, we found that the pattern correlation of amplitude is higher in precipitation amount and frequency (0.64 and 0.63, respectively) than in intensity (0.54).

Figure 5 shows the S1 + S2 cycles of convective and stratiform rainfall occurrence, from the reference. As expected, convective exhibits a stronger diurnal variation on the same grid, although the likelihood of occurrence of stratiform is higher according to non-normalized amplitude values (not shown). This means that subdaily precipitation variations are primarily attributable to the occurrence of convective precipitation. It can be inferred that bias in rainfall amounts, and also incorrect detection of rainfall type, can contribute to errors in satellite-based precipitation.

3.3 | Time–longitude precipitation

We further investigate S1 and S2 precipitation cycles using the time–longitude cross-section (Hovmöller diagram) of precipitation rate (mm h^{-1}) along the latitude band within the two selected sub-regions as delineated in Figure 1. Figure 6 shows the region between 37.5° and 42.5°N, which extends from the Rockies in the west to the Appalachians in the east. The most significant diurnal precipitation variation in

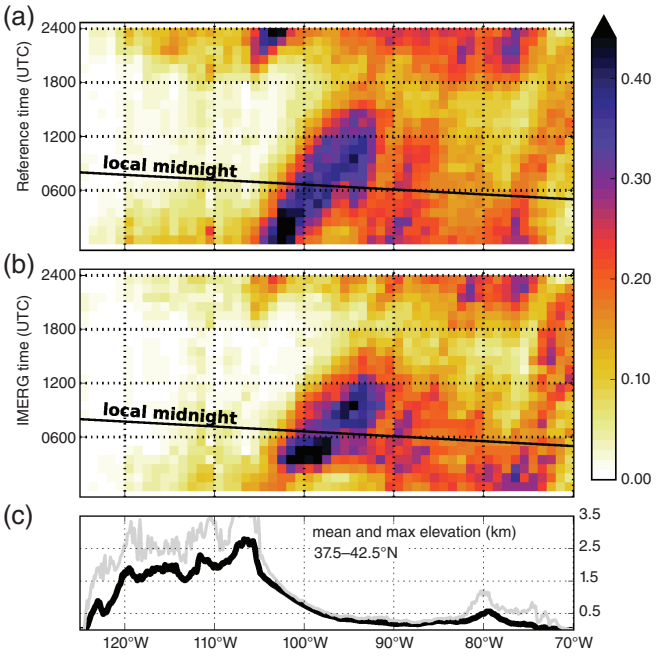

FIGURE 6 Time–longitude diagram of diurnal precipitation variation (mm hr^{-1}) averaged over the selected area of 37.5 –42.5°N and 125.0–70.0°W (i.e. A1 of Figure 1) derived from (a) the reference and (b) IMERG. Time is UTC. The mean and maximum elevations (black and grey lines, respectively) over the latitudinal zone are given in (c)

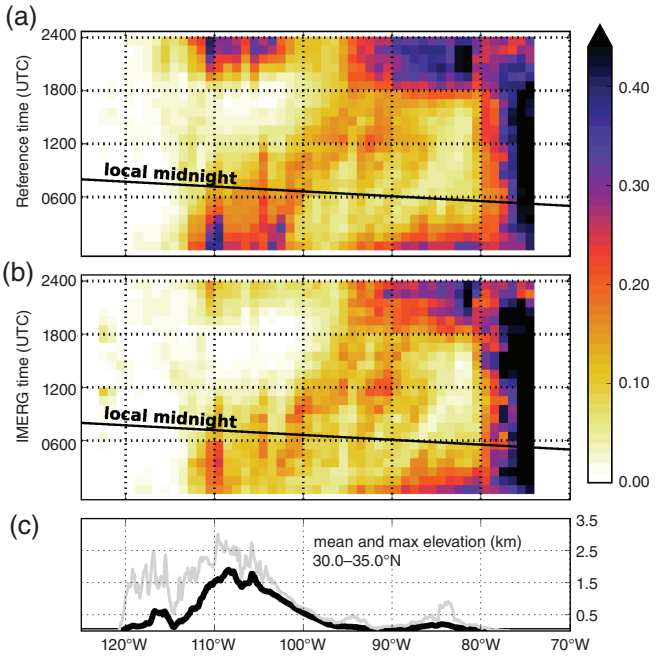

FIGURE 7 As Figure 6, but for the area of 30.0–35.0°N and 125.0–70.0°W (i.e. A2 of Figure 1)

the region is over the Great Plains as a shift of the phase with longitude associated with the eastward propagation of the long-lived MCSs from evening to early morning (also Figure 3).

In Figure 6, we can see that both IMERG and the reference appear to describe the late-afternoon maximum around 105°W, indicating that the MCSs originate from the leeside of the Rockies and delay the timing of the diurnal peaks until around 90°W. As a major source of summer rainfall for the central US, the MCSs have been studied extensively (Carbone & Tuttle, 2008; Geerts et al., 2017; Houze, 2004; Tao et al., 2013). The interested reader is directed to Carbone and Tuttle (2008), who explain the nocturnal rainfall maximum over the Great Plains by the threefold circumstance of self-sustaining organized convection, the mountain–plain solenoid (MPS) ascent, and the Gulf of California low-level jet (GCLLJ).

We found two major differences between IMERG and the reference with respect to the diurnal variation of the region: first, IMERG tends to underestimate precipitation maxima in mountains, and second, the propagating MCSs described by IMERG move faster (i.e. have an early bias) than those in the reference. This data discrepancy will be discussed in detail in section 4.

Figure 7 illustrates the time–longitude map of precipitation in the region between 30° and 35°N (Figure 1). The region shows the diurnal signature of MCSs, although characterized by weaker amplitudes, in the longitudinal band 100°–90°W. On the other hand, the S1 precipitation maxima are observed during late afternoons/early evenings west of ∼ 100°W and east of ∼ 95°W; the former seems to be due to local rainfall events over the Rockies, while the latter is related to the strong moisture transport from the Gulf of Mexico. The local diurnal maxima in the eastern part are coincident with the nocturnal diurnal maxima of the MCSs; consequently, we can see a relatively strong S2 signal over the 100°–90°W longitudinal range (Carbone and Tuttle, 2008; Laing, Carbone, & Levizzani, 2011; also Figure 2). This can also explain the noisy spatial pattern (i.e. converging arrows) of S1 phases, found in Figure 3, for the corresponding region, demonstrating the occurrence of phase superposition. However, according to Figure 4, the amplitude of the S2 resulting from the superposition of S1 cycles is comparatively small. In summary, IMERG-derived diurnal precipitation cycles have discernable resemblance to those of the reference in terms of time–longitude display, although we can observe that biases in the amplitude and phase vary by region.

4 | BIASES IN THE DIURNAL CYCLE OF PRECIPITATION

4.1 | Amplitude

Figure 8 shows the difference in normalized amplitudes between IMERG and the reference diurnal (S1 + S2) precipitation cycle. The difference is defined as a ratio of the normalized amplitude of IMERG to the normalized amplitude of the reference; a positive bias (IMERG peaks higher than reference) is shown in red, while a negative bias (IMERG peaks lower than reference) is shown in blue. The comparison shows that the IMERG performs differently between regions. For instance, the most significant positive bias of IMERG is observed in the central US, including the MCS region

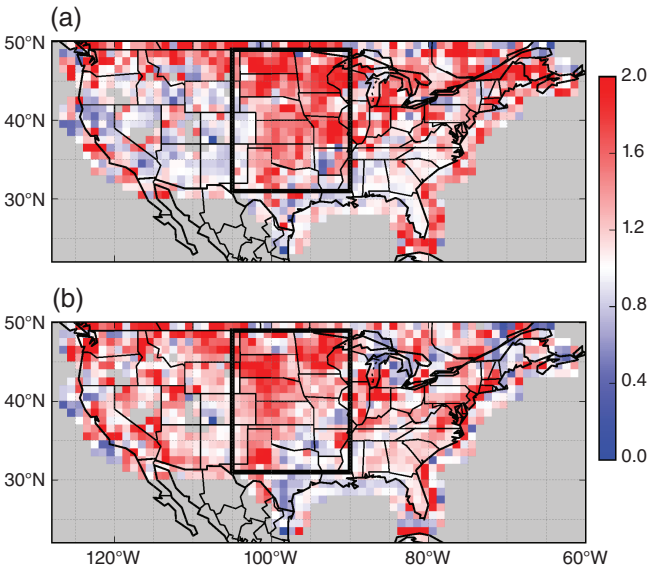

FIGURE 8 Difference in normalized amplitude of (S1 + S2) precipitation cycle between IMERG and reference (i.e. IMERG divided by the reference) in terms of precipitation (a) amount, and (b) frequency. Red denotes IMERG peaks higher than the reference, while blue IMERG peaks lower than the reference. The black box shows the MCS region

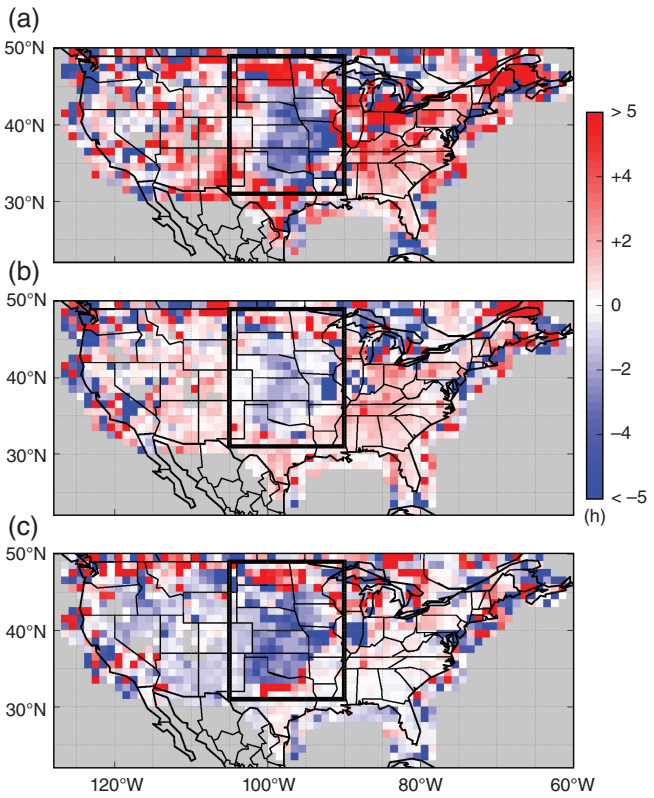

FIGURE 9 Difference in peak time of (S1 + S2) precipitation cycles between IMERG and reference (i.e. IMERG minus reference) in terms of (a) amount and (b) frequency. (c) shows the difference in phase peak time of occurrence (convective minus stratiform precipitation types). Red means IMERG (or convective) peaks later than the reference (stratiform), while blue means IMERG (or convective) peaks earlier than the reference (stratiform). The black box shows the MCS region

(black box of Figure 8). Given that the MCS is a collection of storms which subsequently self-regenerate while the system moves eastward, one possible explanation is that IMERG overestimates deep convection/ice components at the mature stage and detects precipitation even from the ice remaining at the decaying stage (i.e. false alarms from non-precipitating hydrometeors). This can lead to overestimation of both the amount and frequency of the IMERG-derived precipitation cycles.

On the other hand, relatively weaker diurnal variations of precipitation amount are found in IMERG over mountain regions (Figure 8). Such complex topography is challenging for satellite precipitation retrievals (Cattani, Merino, & Levizzani, 2016; Dinku, Chidzambwa, Ceccato, Connor, & Ropelewski, 2008; Dinku, Ceccato, & Connor, 2011; Kim et al., 2017). For the Appalachian region of the eastern US, IMERG tends to slightly underestimate both precipitation amount and frequency, which can be related to orographically enhanced clouds. The satellite poorly estimates the precipitation rates from those warm clouds because they are generally associated with low ice content and higher brightness temperature. For example, Dinku et al. (2008) studied the poor performance of satellites over the complex terrain of Ethiopia and suggested that satellites may not detect the warm clouds since they would be too warm for IR thresholds and there is not much ice to be detected by PMW sensors. Warm orographic rains are thus likely to be underestimated by satellite observation (also Shige, Kida, Ashiwake, Kubota, & Aonashi, 2013). Duan, Wilson, and Barros (2015) also investigated the precipitation radar QPE by the TRMM in the southern Appalachian Mountains and found that precipitation of small-scale systems and isolated deep convection tends to be underestimated due to spatial averaging at the radar resolution. These explanations could also be applied to the underestimated precipitation maxima over the complex topography in the western US. Interestingly, however, IMERG slightly overestimates the frequency of precipitation maxima. For instance, the background surface emissivity from snow cover over the high mountains, which often produces false precipitation events, can bring unexpected errors to the PMW estimation.

4.2 | Timing of precipitation maxima

This subsection examines the phase of the diurnal cycles (S1 + S2) between IMERG and the reference (Figure 9). Although interpretation of peak time differences is less certain over the areas in where the diurnal variations cannot be explained by only the two harmonics, the peak time for IMERG tends to appear slightly later than that of the reference in most areas, except the central US. As a result, large-scale spatial patterns are observed over the MCS region (black box of Figure 9); late biases appear on the west side versus early biases on the east. Note that similar patterns are found from the comparison of peak time between convective and stratiform precipitation as seen in Figure 9c, i.e. stratiform

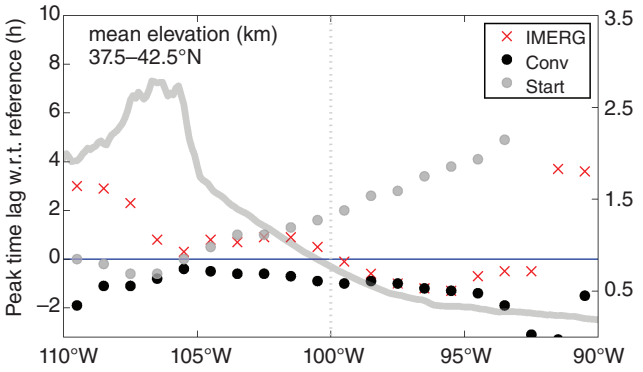

FIGURE 10 Precipitation peak time of the S1 harmonic of IMERG, convective, and stratiform precipitation relative to that of the reference along longitude from 110 to 90°W over A1 (Figure 1)

precipitation peaks later by less than 1 h in general, however the peak time lag gradually increases as one moves from west to east across the region.

This can be explained by the MCS life cycle. The system begins with convective elements at the genesis phase and then produces stratiform precipitation regions in the later phases (Houze, 2004). Thus, we can see that a stratiform diurnal cycle peaks a few hours after the convective maximum, particularly in the MCS dissipation area (east to around 95.0°W). Such mixed-phase cloud systems can directly affect the performance of satellite precipitation observations. For example, Yamamoto, Furuzawa, Higuchi, and Nakamura (2008) investigated the peak time between the sensors on board the TRMM satellite and found that systematic peak time differences among the sensors are related to the evolution of convective precipitation. They inferred that the radar (PR) detects near-surface rain from the initial to mature stages of the convective precipitation and the microwave imager (TMI) is more sensitive to heavy rain with solid hydrometeors during the mature stage of convective precipitation, while the infrared scanner (VIRS) detects deep convective clouds at the mature and decaying stages.

Although tracking the sensitivity of each sensor involved in IMERG to cloud systems is beyond the scope of this article, we can assume that IMERG is primarily influenced by the PMW sensors which are the backbone of the GPM constellation; hence, it is primarily influenced by convection during the mature stage of the system life cycle. As a result, IMERG shows a better (more sensitive) performance in detecting the convective precipitation than in observing co-existing stratiform precipitation within the MCS, given that the area of large ice particles lifted by strong updraughts in convective cores leads to lower brightness temperatures for the satellite PMW retrievals.

To verify this assumption, we compare the phase of diurnal cycle for selected precipitation features at each 1° of longitude between 110°W and 90°W within Area 1 (Figure 1). Figure 10 shows the peak time of IMERG, convective, and stratiform as a function of time lag with respect to the peak time of the reference. West of 100°W, IMERG shows a common late bias compared to reference, which can be attributed to either shallow orographic clouds with low ice concentration or small-scale local convective clouds, i.e. IMERG may observe the latter stages of the cloud life cycle only after they are sufficiently mature. Meanwhile, east of 100°W, the stratiform maximum appears to gradually lag behind the convective maximum as the MCSs become increasingly dominated by the (trailing) stratiform region during its life cycle while the system is moving eastward; eventually the peak of convective precede that of stratiform precipitation by up to 6 h at around 93°W. The peak time in the reference (blue line in Figure 10) can be found somewhere between the convective and stratiform maxima, although it is still closer to that of convective. By contrast, however, the peak time in IMERG more closely follows that of convective precipitation as IMERG PMW estimates are biased toward the leading convective part and ice content aloft. As a consequence, IMERG precipitation estimates have notable biases in the phase of the diurnal cycle over the area of propagating MCSs.

5 | SUMMARY AND CONCLUSIONS

We have evaluated the diurnal variations of summer precipitation derived from IMERG over the CONUS using the ground reference derived from the MRMS radar-based precipitation data. For the evaluation, we computed the diurnal and semidiurnal (S1 and S2) cycles from IMERG and the reference on a 1°/1 h scale and compared the normalized amplitude and phase of diurnal cycles in terms of precipitation amount, frequency, and intensity.

IMERG shows overall good agreement with the reference in terms of both S1 and S2 cycles. We have found that IMERG agrees well in terms of a large-scale spatial pattern of diurnal variations in precipitation, as well as in terms of distinct local diurnal characteristics which are probably related to surface boundary forcing (e.g. land–sea or mountain–valley breezes), although the scarcity of precipitation in the western US makes the interpretation of harmonics challenging. Additionally, the comparison of the Hovmöller diagrams in the two selected regions shows that the shape of the IMERG-estimated diurnal cycles has a discernable resemblance to that of the reference, and consequently IMERG captures fairly well the typical S1 and S2 characteristics of the US summer precipitation. The evaluation results demonstrate that the IMERG precipitation estimates can be a reliable alternative to ground-based measurements, even at the subdaily scale; however, region-specific discrepancies still remain.

The significant contribution of convective rainfall to the diurnal variations of precipitation implies that the weak linkage between the satellite precipitation retrievals and precipitation type information may account for the regional biases in IMERG. Indeed, the convective/stratiform partitioning data from the reference allow us to confirm that

the different diurnal phases of the two different precipitation types co-exciting within the MCSs can make IMERG out of phase with the reference over the central US. Over mountainous regions, we suspect that orographic precipitation and local convective precipitation can lead to the negative bias (underestimation in terms of diurnal maxima) observed in IMERG, although additional factors (e.g. complex topography, snow cover) make the interpretation of biases difficult.

The results from this study should be carefully addressed before using IMERG data, for example to investigate precipitation processes or to validate the performance of models based on the IMERG data, with a focus on diurnal variations in precipitation. This is particularly the case at the local and regional level. Note that this study is concerned with the IMERG Final run which is corrected by monthly gauge analysis. However, the results can be generalized to uncalibrated IMERG (satellite-only estimates), since normalized amplitude and diurnal phase are quantities that are not affected by the correction.

Furthermore, the results can be adopted as a benchmark for the next versions of the IMERG; the IMERG version 05 is planned for release during 2017. This work can be extended to other seasons. For example, we expect that the western US will show a strong diurnal signal during winter for the evaluation of the IMERG over coastal areas. Also, this approach can be easily applied to other regions where MCSs are reported (Anabor, Stensrud, & de Moraes, 2008; Laing, Carbone, Levizzani, & Tuttle, 2008; Laing et al., 2011; Stensrud, 1996) and a reliable ground reference exists. Most importantly, our findings suggest that the most fundamental improvement of satellite precipitation retrieval requires a better understanding of the relationship between cloud processes and surface precipitation, e.g. the budget of integrated ice content and precipitation as a function of the MCS life stage.

ACKNOWLEDGEMENTS

The study was funded by the Austrian Science Fund (FWF) under research grant W 1256-G15 (Doctoral Programme Climate Change Uncertainties, Thresholds and Coping Strategies). Sungmin O would like to express her thanks to Prof. Yang Hong for the opportunity of a research stay at the University of Oklahoma. The IMERG data are provided by the NASA/Goddard Space Flight Center's PMM and PSS teams through http://pmm.nasa.gov/data-access/downloads/gpm (accessed 16 December 2017).

REFERENCES

Anabor, V., Stensrud, D.J. and de Moraes, O. (2008) Serial upstream-propagating mesoscale convective system events over Southeastern South America. *Monthly Weather Review*, 136, 3087–3105. https://doi.org/10.1175/2007MWR2334.1.

Artan, G., Gadain, H., Smith, J.L., Asante, K., Bandaragoda, C.J. and Verdin, J.P. (2007) Adequacy of satellite-derived rainfall data for streamflow modeling. *Natural Hazards*, 43, 167–185. https://doi.org/10.1007/s11069-007-9121-6.

Carbone, R.E. and Tuttle, J.D. (2008) Rainfall occurrence in the US warm season: The diurnal cycle. *Journal of Climate*, 21, 4132–4146. https://doi.org/10.1175/2008JCLI2275.1.

Cattani, E., Merino, A. and Levizzani, V. (2016) Evaluation of monthly satellite-derived precipitation products over East Africa. *Journal of Hydrometeorology*, 17, 2555–2573. https://doi.org/10.1175/JHM-D-15-0042.1.

Clark, A.J., Gallus, W.A. and Chen, T.C. (2007) Comparison of the diurnal precipitation cycle in convection-resolving and non-convection-resolving mesoscale models. *Monthly Weather Review*, 135, 3456–3473. https://doi.org/10.1175/MWR3467.1.

Dai, A. (2001) Global precipitation and thunderstorm frequencies. Part II: Diurnal variations. *Journal of Climate*, 14, 1112–1128. https://doi.org/10.1175/1520-0442(2001)0141112:gpatfp2.0.CO;2.

Dai, A., Giorgi, F. and Trenberth, K.E. (1999) Observed and model-simulated diurnal cycles of precipitation over the contiguous United States. *Journal of Geophysical Research Atmospheres*, 104, 6377–6402.

Dinku, T., Ceccato, P. and Connor, S.J. (2011) Challenges of satellite rainfall estimation over mountainous and arid parts of east Africa. *International Journal of Remote Sensing*, 32, 5965–5979. https://doi.org/10.1080/01431161.2010.499381.

Dinku, T., Chidzambwa, S., Ceccato, P., Connor, S.J. and Ropelewski, C.F. (2008) Validation of high-resolution satellite rainfall products over complex terrain. *International Journal of Remote Sensing*, 29, 4097–4110. https://doi.org/10.1080/01431160701772526.

Duan, Y., Wilson, A.M. and Barros, A.P. (2015) Scoping a field experiment: Error diagnostics of TRMM precipitation radar estimates in complex terrain as a basis for IPHEx2014. *Hydrology and Earth System Sciences*, 19, 1501–1520. https://doi.org/10.5194/hess-19-1501-2015.

Fenta, A.A., Rientjes, T., Haile, A.T. and Reggiani, P.Melesse AM, Abtew W and Setegn SG. (Eds.) (2014) Satellite rainfall products and their reliability in the Blue Nile Basin *Nile River Basin*. Cham, Switzerland: Springer, pp. 51–67. https://doi.org/10.1007/978-3-319-02720-3_4.

Gebregiorgis, A.S., Kirstetter, P.E., Hong, Y.E., Carr, N.J., Gourley, J.J., Petersen, W. and Zheng, Y. (2017) Understanding overland multisensor satellite precipitation error in TMPA-RT products. *Journal of Hydrometeorology*, 18, 285–306. https://doi.org/10.1175/JHM-D-15-0207.1.

Geerts, B., Parsons, D., Ziegler, C.L., Weckwerth, T.M., Biggerstaff, M.I., Clark, R.D., Coniglio, M.C., Demoz, B.B., Ferrare, R.A., Gallus, W.A., Haghi, K., Hanesiak, J.M., Klein, P.M., Knupp, K.R., Kosiba, K., McFarquhar, G.M., Moore, J.A., Nehrir, A.R., Parker, M.D., Pinto, J.O., Rauber, R.M., Schumacher, R.S., Turner, D.D., Wang, Q., Wang, X., Wang, Z. and Wurman, J. (2017) The 2015 plains elevated convection at night field project. *Bulletin of the American Meteorological Society*, 98, 767–786. https://doi.org/10.1175/BAMS-D-15-00257.1.

He, X., Kim, H., Kirstetter, P.E., Yoshimura, K., Chang, E.C., Ferguson, C.R., Erlingis, J.M., Hong, Y. and Oki, T. (2015) The diurnal cycle of precipitation in regional spectral model simulations over West Africa: Sensitivities to resolution and cumulus schemes. *Weather and Forecasting*, 30, 424–445. https://doi.org/10.1175/WAF-D-14-00013.1.

Hong, Y., Adler, R. and Huffman, G. (2006) Evaluation of the potential of NASA multi-satellite precipitation analysis in global landslide hazard assessment. *Geophysical Research Letters*, 33, L22402. https://doi.org/10.1029/2006GL028010.

Hong, Y., Adler, R.F., Hossain, F., Curtis, S. and Huffman, G.J. (2007) A first approach to global runoff simulation using satellite rainfall estimation. *Water Resources Research*, 43, W08502. https://doi.org/10.1029/2006WR005739.

Hong, Y., Hsu, K.L., Sorooshian, S. and Gao, X. (2004) Precipitation estimation from remotely sensed imagery using an artificial neural network cloud classification system. *Journal of Applied Meteorology and Climatology*, 43, 1834–1853. https://doi.org/10.1175/JAM2173.1.

Hou, A.Y., Kakar, R.K., Neeck, S., Azarbarzin, A.A., Kummerow, C.D., Kojima, M., Oki, R., Nakamura, K. and Iguchi, T. (2014) The Global Precipitation Measurement mission. *Bulletin of the American Meteorological Society*, 95, 701–722. https://doi.org/10.1175/BAMS-D-13-00164.1.

Houze, R.A. (2004) Mesoscale convective systems. *Reviews of Geophysics*, 42, RG4003. https://doi.org/10.1029/2004RG000150.

Huang, W.R. and Chan, J.C.L. (2011) Maintenance mechanisms for the early-morning maximum summer rainfall over southeast China. *Quarterly*

Journal of the Royal Meteorological Society, 137, 959–968. https://doi.org/10.1002/qj.815.

Huffman, G.J., Bolvin, D.T., Braithwaite, D., Hsu, K., Joyce, R., Kidd, C., Nelkin, E.J. and Xie, P. (2015a) *NASA Global Precipitation Measurement (GPM) Integrated Multi-satellitE Retrievals for GPM (IMERG)*, Algorithm Theoretical Basis Document version 4.5, NASA/GSFC, Greenbelt, MD.

Huffman, G.J., Bolvin, D.T. and Nelkin, E.J. (2015b) *Integrated Multi-satellitE Retrievals for GPM (IMERG) technical documentation*. Greenbelt, MD: NASA/GSFC.

Huffman, G.J., Bolvin, D.T., Nelkin, E.J., Wolff, D.B., Adler, R.F., Gu, G., Hong, Y., Bowman, K.P. and Stocker, E.F. (2007) The TRMM Multisatellite Precipitation Analysis (TMPA): Quasi-global, multiyear, combined-sensor precipitation estimates at fine scales. *Journal of Hydrometeorology*, 8, 38–55. https://doi.org/10.1175/JHM560.1.

Joyce, R.J. and Xie, P. (2011) Kalman filter-based CMORPH. *Journal of Hydrometeorology*, 12, 1547–1563. https://doi.org/10.1175/JHM-D-11-022.1.

Kim, K., Park, J., Baik, J. and Choi, M. (2017) Evaluation of topographical and seasonal feature using GPM IMERG and TRMM 3b42 over Far-East Asia. *Atmospheric Research*, 187, 95–105. https://doi.org/10.1016/j.atmosres.2016.12.007.

Kirstetter, P.E., Hong, Y., Gourley, J.J., Chen, S., Flamig, Z., Zhang, J., Schwaller, M., Petersen, W. and Amitai, E. (2012) Toward a framework for systematic error modeling of spaceborne precipitation radar with NOAA/NSSL ground radar-based National Mosaic QPE. *Journal of Hydrometeorology*, 13, 1285–1300. https://doi.org/10.1175/JHM-D-11-0139.1.

Kirstetter, P.E., Hong, Y., Gourley, J.J., Schwaller, M., Petersen, W. and Zhang, J. (2013) Comparison of TRMM 2a25 products, version 6 and version 7, with NOAA/NSSL ground radar-based National Mosaic QPE. *Journal of Hydrometeorology*, 14, 661–669. https://doi.org/10.1175/JHM-D-12-030.1.

Kirstetter, P.E., Hong, Y., Gourley, J.J., Cao, Q., Schwaller, M. and Petersen, W. (2014) A research framework to bridge from the Global Precipitation Measurement mission core satellite to the constellation sensors using ground radar-based National Mosaic QPE. In: L. Venkataraman, V. Lakshmi, D. Alsdorf, M. Anderson, S. Biancamaria, M. Cosh, J. Entin, G. Huffman, W. Kustas, P. van Oevelen, T. Painter, J. Parajka, M. Rodell and C. Rüdiger (Eds.) *Remote sensing of the terrestrial water cycle, AGU books Geophysical Monograph Series, Chapman monograph on remote sensing*. Hoboken, NJ: John Wiley & Sons. https://doi.org/10.1002/9781118872086.ch4.

Koo, M.-S. and Hong, S.-Y. (2010) Diurnal variations of simulated precipitation over East Asia in two regional climate models. *Journal of Geophysical Research*, 115, D05105. https://doi.org/10.1029/2009JD012574.

Laing, A.G., Carbone, R.E. and Levizzani, V. (2011) Cycles and propagation of deep convection over equatorial Africa. *Monthly Weather Review*, 139, 2832–2853. https://doi.org/10.1175/2011MWR3500.1.

Laing, A.G., Carbone, R., Levizzani, V. and Tuttle, J. (2008) The propagation and diurnal cycles of deep convection in northern tropical Africa. *Quarterly Journal of the Royal Meteorological Society*, 134, 93–109. https://doi.org/10.1002/qj.194.

Le, M., Chandrasekar, V. and Biswas, S. (2016) Evaluation and validation of GPM dual-frequency classification module after launch. *Journal of Atmospheric and Oceanic Technology*, 33, 2699–2716. https://doi.org/10.1175/JTECH-D-15-0253.1.

Li, L., Hong, Y., Wang, J., Adler, R.F., Policelli, F.S., Habib, S., Irwn, D., Korme, T. and Okello, L. (2009) Evaluation of the real-time TRMM-based multi-satellite precipitation analysis for an operational flood prediction system in Nzoia Basin, Lake Victoria, Africa. *Natural Hazards*, 50, 109–123. https://doi.org/10.1007/s11069-008-9324-5.

Li, N., Tang, G., Zhao, P., Hong, Y., Gou, Y. and Yang, K. (2017) Statistical assessment and hydrological utility of the latest multi-satellite precipitation analysis IMERG in Ganjiang River basin. *Atmospheric Research*, 183, 212–223. https://doi.org/10.1016/j.atmosres.2016.07.020.

Li, X.H., Zhang, Q. and Xu, C.Y. (2012) Suitability of the TRMM satellite rainfalls in driving a distributed hydrological model for water balance computations in Xinjiang catchment, Poyang lake basin. *Journal of Hydrology*, 426–427, 28–38. https://doi.org/10.1016/j.jhydrol.2012.01.013.

Liang, X.Z. (2004) Regional climate model simulation of summer precipitation diurnal cycle over the United States. *Geophysical Research Letters*, 31, L24208. https://doi.org/10.1029/2004GL021054.

Nesbitt, S.W. and Zipser, E.J. (2003) The diurnal cycle of rainfall and convective intensity according to three years of TRMM measurements. *Journal of Climate*, 16, 1456–1475. https://doi.org/10.1175/1520-0442-16.10.1456.

Oki, T. and Musiake, K. (1994) Seasonal change of the diurnal cycle of precipitation over Japan and Malaysia. *Journal of Applied Meteorology and Climatology*, 33, 1445–1463. https://doi.org/10.1175/1520-0450(1994)0331445:scotdc2.0.CO;2.

Prakash, S., Mitra, A.K., AghaKouchak, A., Liu, Z., Norouzi, H. and Pai, D. (2016) A preliminary assessment of GPM-based multi-satellite precipitation estimates over a monsoon dominated region. *Journal of Hydrology*. https://doi.org/10.1016/j.jhydrol.2016.01.029. (in press).

Pu, Z., Tao, W.K., Braun, S., Simpson, J., Jia, Y., Halverson, J., Olson, W. and Hou, A. (2002) The impact of TRMM data on mesoscale numerical simulation of supertyphoon. *Monthly Weather Review*, 130, 2448–2458. https://doi.org/10.1175/1520-0493(2002)1302448:tiotdo2.0.CO;2.

Shige, S., Kida, S., Ashiwake, H., Kubota, T. and Aonashi, K. (2013) Improvement of TMI rain retrievals in mountainous areas. *Journal of Applied Meteorology and Climatology*, 52, 242–254. https://doi.org/10.1175/JAMC-D-12-074.1.

Skofronick-Jackson, G., Petersen, W.A., Berg, W., Kidd, C., Stocker, E.F., Kirschbaum, D.B., Kakar, R., Braun, S.A., Huffman, G.J., Iguchi, T., Kirstetter, P.E., Kummerow, C., Meneghini, R., Oki, R., Olson, W.S., Takayabu, Y.N., Furukawa, K. and Wilheit, T. (2017) The Global Precipitation Measurement (GPM) mission for science and society. *Bulletin of the American Meteorological Society*, 98, 1679–1695. https://doi.org/10.1175/BAMS-D-15-00306.1.

Stensrud, D.J. (1996) Importance of low-level jets to climate: A review. *Journal of Climate*, 9, 1698–1711. https://doi.org/10.1175/1520-0442(1996)0091698:iolljt2.0.CO;2.

Sungmin, O., Foelsche, U., Kirchengast, G., Fuchsberger, J., Tan, J. and Petersen, W.A. (2017) Evaluation of GPM IMERG Early, Late, and Final rainfall estimates using WegenerNet gauge data in southeastern Austria. *Hydrol. Earth Syst. Sci.*, 21, 6559-6572. https://doi.org/10.5194/hess-21-6559-2017.

Surcel, M., Berenguer, M. and Zawadzki, I. (2010) The diurnal cycle of precipitation from continental radar mosaics and numerical weather prediction models. Part I: Methodology and seasonal comparison. *Monthly Weather Review*, 138, 3084–3106. https://doi.org/10.1175/2010MWR3125.1.

Tan, J., Petersen, W.A. and Tokay, A. (2016) A novel approach to identify sources of errors in IMERG for GPM ground validation. *Journal of Hydrometeorology*, 17, 2477–2491. https://doi.org/10.1175/JHM-D-16-0079.1.

Tang, G., Ma, Y., Long, D., Zhong, L. and Hong, Y. (2016) Evaluation of GPM Day-1 IMERG and TMPA Version-7 legacy products over mainland China at multiple spatiotemporal scales. *Journal of Hydrology*, 533, 152–167. https://doi.org/10.1016/j.jhydrol.2015.12.008.

Tao, W., Wu, D., Matsui, T., Peters-Lidard, C., Lang, S., Hou, A., Rienecker, M., Petersen, W. and Jensen, M. (2013) Precipitation intensity and variation during MC3e: A numerical modeling study. *Journal of Geophysical Research Atmospheres*, 118, 7199–7218. https://doi.org/10.1002/jgrd.50410.

Tian, B., Held, I.M., Lau, N.-C. and Soden, B.J. (2005) Diurnal cycle of summertime deep convection over North America: A satellite perspective. *Journal of Geophysical Research*, 110, D08108. https://doi.org/10.1029/2004JD005275.

Tian, Y., Peters-Lidard, C.D., Choudhury, B.J. and Garcia, M. (2007) Multitemporal analysis of TRMM-based satellite precipitation products for land data assimilation applications. *Journal of Hydrometeorology*, 8, 1165–1183. https://doi.org/10.1175/2007JHM859.1.

Wang, J. and Wolff, D.B. (2010) Evaluation of TRMM ground-validation radar-rain errors using rain gauge measurements. *Journal of Applied Meteorology and Climatology*, 49, 310–324. https://doi.org/10.1175/2009JAMC2264.1.

Yamamoto, M.K., Furuzawa, F.A., Higuchi, A. and Nakamura, K. (2008) Comparison of diurnal variations in precipitation systems observed by TRMM PR, TMI, and VIRS. *Journal of Climate*, 21, 4011–4028. https://doi.org/10.1175/2007JCLI2079.1.

Yin, S., Chen, D. and Xie, Y. (2009) Diurnal variations of precipitation during the warm season over China. *International Journal of Climatology*, 29, 1154–1170. https://doi.org/10.1002/joc.1758.

Zeweldi, D.A. and Gebremichael, M. (2009) Evaluation of CMORPH precipitation products at fine space-time scales. *Journal of Hydrometeorology*, 10, 300–307. https://doi.org/10.1175/2008JHM1041.1.

Zhang, J., Howard, K., Langston, C., Kaney, B., Qi, Y., Tang, L., Grams, H., Wang, Y., Cocks, S., Martinaitis, S., Arthur, A., Cooper, K., Brogden, J. and Kitzmiller, D. (2016) Multi-Radar Multi-Sensor (MRMS) quantitative precipitation estimation: Initial operating capabilities. *Bulletin of the American Meteorological Society*, 97, 621–638. https://doi.org/10.1175/BAMS-D-14-00174.1.

Zhang, J., Qi, Y., Howard, K., Langston, C. and Kaney, B. (2011) *Radar Quality Index (RQI) – A combined measure of beam blockage and VPR effects in a national network*. Proceedings of the Eighth International Symposium on Weather Radar and Hydrology, Exeter, England, Royal Meteorological Society

Zhou, Y., Lau, W.K.M. and Huffman, G.J. (2015) Mapping TRMM TMPA into average recurrence interval for monitoring extreme precipitation events. *Journal of Applied Meteorology and Climatology*, 54, 979–995. https://doi.org/10.1175/JAMC-D-14-0269.1.

Zhou, T., Yu, R., Chen, H., Dai, A. and Pan, Y. (2008) Summer precipitation frequency, intensity, and diurnal cycle over China: A comparison of satellite data with rain gauge observations. *Journal of Climate*, 21, 3997–4010. https://doi.org/10.1175/2008JCLI2028.1.

How to cite this article: S. O, P.-E. Kirstetter, Evaluation of diurnal variation of GPM IMERG derived summer precipitation over the contiguous US using MRMS data. *Q J R Meteorol Soc.* 2018;144:270–281. https://doi.org/10.1002/qj.3218.